# Supercritical $CO_2$ Effects on Calcite Wettability: A Molecular Perspective

Tran Thi Bao Le and Alberto Striolo*

*Department of Chemical Engineering, University College London, London WC1E 6BT United Kingdom*

David R. Cole

*School of Earth Sciences, The Ohio State University, Columbus, Ohio 43210 United States of America*

## ABSTRACT

The wettability behaviour of reservoir rocks plays a vital role in determining $CO_2$ storage capacity and containment security. Several experimental studies characterised the wettability of $CO_2$/brine/rock systems for a wide range of realistic conditions. To develop a fundamental understanding of the molecular mechanisms responsible for such observations, the results of molecular dynamics simulations, conducted at atomistic resolution, are reported here for representative systems in a wide range of pressure and temperature conditions. Several force fields are considered, achieving good agreement with experimental data for the structure of interfacial water, but only partial agreement in terms of contact angles. In general, the results suggest that, at the conditions chosen, water strongly wet calcite, resulting in water contact angles either too low to be determined accurately with the algorithms implemented here, or up to ~46º, depending on the force field implemented. These values are in agreement with some, but not all experimental data available in the literature, some of which report contact angles as high as 90º. One supercritical $CO_2$ droplet was simulated in proximity of the wet calcite surface. The results show pronounced effects due to salinity, which are also dependent on the force field implemented to describe the solid substrate. When the force field predicts complete water wettability, increasing NaCl salinity seems to slightly increase the calcite affinity for $CO_2$, monotonically as the NaCl concentration increases, because of the preferential adsorption of salt ions at the water-rock interface. When the other force field was implemented, it was not possible to quantify salt effects, but the simulations suggested strong interactions between the supercritical $CO_2$ droplet and the second hydration layer on calcite. The results presented could be relevant for predicting the longevity of $CO_2$ sequestration in geological repositories.

* Author to whom correspondence should be addressed: a.striolo@ucl.ac.uk

**Keywords**: Wettability; Contact angle; Calcite; Salt; Molecular dynamics

## 1. INTRODUCTION

Geologic carbon sequestration (GCS) into natural formations (e.g., deep saline aquifers, un-mineable coal beds, and depleted oil/gas reservoirs) is one among several technologies that could contribute to reduce anthropogenic $CO_2$ from the atmosphere. GCS involves the capture of $CO_2$ from emitters, or perhaps directly from air, followed by injection of the captured $CO_2$ into geological reservoirs for long-term storage. Geologic $CO_2$ storage in deep saline aquifers presents several advantages compared to other kinds of subsurface repositories.[1-2] It has been estimated that deep saline aquifers offer the largest potential capacity for $CO_2$ storage, up to 10,000 Gt $CO_2$.[2-3] Such potential repositories are widely distributed and they are frequently located close to stationary point-source $CO_2$ emission sites.[3]

The injection of $CO_2$ into subsurface reservoirs results in chemical and physical processes that could govern the long-term storage potential and its security.[2, 4] When injection ceases, supercritical $CO_2$ could be trapped as an immiscible free phase and as a solute in the aqueous phase within the porous rocks.[5] Various physicochemical storage mechanisms have been identified that could prevent the upward migration, and ultimately the leakage, of the injected $CO_2$. Such processes include: structural trapping,[6] residual trapping,[7] dissolution trapping,[8] and mineral trapping.[9] These mechanisms, and especially structural and residual trapping, are strongly influenced by the wettability characteristics of the mineral phases that come in contact with aqueous brines and injected $CO_2$.[6, 10-11] Wettability describes the adhesion, or spread, of a fluid on a solid substrate in the presence of other immiscible fluids. Increased $CO_2$ wettability of cap rocks at storage conditions substantially lowers the structural trapping capacity,[6, 10] and the residual trapping of $CO_2$ in mixed-wet rocks is significantly reduced relative to trapping in water-wet systems.[11-12] These examples demonstrate the vital importance of wettability of the reservoir rocks in estimating storage capacity of a formation and assessing its longevity (i.e., the potential of $CO_2$ leakage to the surface). Moreover, wettability also affects morphology and interfacial areas,[13] capillary pressure, as well as transport and distribution of reservoir fluids.[14]

The three-phase contact angle at the $CO_2$-brine-mineral interface, $\theta$, is often used to evaluate wettability of a rock surface. The contact angle is described by the Young's equation:[15]

$$\cos\theta = \frac{\gamma_{S1} - \gamma_{S2}}{\gamma_{12}} \quad (1)$$

In Eq, (1), $\gamma_{S1}$ and $\gamma_{S2}$ are the interfacial tensions between the solid surface and the two fluids, while $\gamma_{12}$ is the interfacial tension between the two fluids. Depending on the balance between intermolecular forces, the contact angle ranges from 0–180°. Complete wetting is defined when $\theta = 0°$, partial wetting when $0 < \theta < 180°$, and nonwetting when $\theta = 180°$.[16] A schematic of the contact angle $\theta$ considered in this work for the $CO_2$-water-mineral system is shown in Figure 1. A number of studies measured contact angles as a function of pressure, temperature, surface chemistry and brine composition, by either experiments or molecular dynamics (MD) simulations.[17-26] For example, Dickson et al.[17] developed a high-pressure apparatus to measure $CO_2$/water/solid contact angles on glass substrates with different

hydrophilicities as quantified by silanol (SiOH) surface density. As the $CO_2$ pressure increased from atmospheric pressure to 61.2 bar at 23°C, the results showed that θ increased from 71° to 99° on the substrate with 37% SiOH, and from 98° to 141° on the substrate with 12% SiOH. Wang et al.[20] measured contact angles on quartz, calcite, microcline, kaolinite, illite, and phlogopite, in a $CO_2$ environment under conditions relevant to GCS. The results show that all the minerals are water-wet (θ < 30°). These studies reported that the temperature and pressure dependence of contact angles exhibit no clear trend for all surfaces, while both pH and ionic strength are good predictors of contact angle. Concerning simulations, Chen et al.[27] found a good agreement between MD simulations and experimental results when they studied water contact angles on quartz in the presence of $CO_2$ at GCS conditions. The water contact angle was found to increase as the ionic strength increased; pressure and temperature were found to have weak effect on contact angle. Other MD simulations suggest that, for water on three silica surfaces,[22] the dependence of θ on pressure and temperature is controlled by the silanol number density on the solid surfaces.

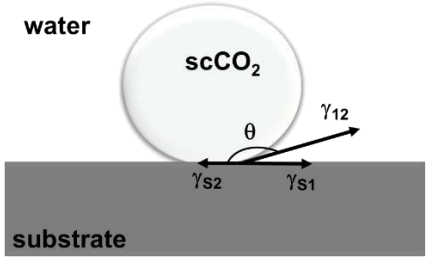


**Figure 1**. Schematic illustrating the contact angle as measured through the $CO_2$ phase. In this example, the mineral substrate is preferentially wet by water.

Porous sandstone and carbonate formations are considered as potential sites for CGS. Most carbonate minerals are composed of limestone and dolostone. Because calcite is the major component in limestone and because it is widely present in geological systems, it is among the most studied minerals. Numerous experiments quantified the wettability of systems composed of calcite, $CO_2$ and brine.[18-20, 28-30] However, the experimental results are somewhat inconsistent regarding the wetting behaviour of calcite as a function of changes in temperature, pressure, and brine composition. For example, Arif et al.[28] measured the water contact angle in calcite/$CO_2$/brine systems as a function of pressure, temperature and salinity for a wide range of conditions. They found that the contact angle increased with pressure and brine salinity and decreased with temperature. On the contrary, Espinoza and Santamarina[18] measured the contact angle at ambient temperature in a wide range of pressures, up to 20 MPa. They reported that the contact angles remained nearly constant as pressure increased, and that dissolved NaCl had no significant effect on the measurements. The findings of Arif et al.[28] seem to be consistent with data obtained by Bikkina et al.,[19] who reported a slight increase of water contact angle as the pressure increased from 1.38 to 5.52 MPa. However, this group reported a reduction in the contact angle at higher pressures (8.27–20.68 MPa). In contrast, Wang et al. [20] reported little dependence of the contact angle on pressure and temperature. It should however be recognised that surface roughness and the possible

presence of organics on natural substrates, both of which are difficult to quantify, are likely to strongly affect contact angle measurements.

Given this inconsistency in the available results, the objective of this study is to develop a molecular-level understanding regarding the wettability of calcite at GCS conditions. To this end, molecular dynamics simulations (MD) are employed at atomistic resolution. Our results complement those recently reported by Silvestri et al.,[31] who performed NVT simulations to compute the contact angle of cylindrical and spherical water droplets on the calcite $[10\bar{1}4]$ surface in $CO_2$ atmosphere at 50° C and 20 MPa. Our work adopts two synergistic approaches. The first concerns the validation of the model implemented to simulate water, to ensure its suitability to describe the system of interest (the water-calcite interface). The second is a systematic investigation concerning the wettability of $CO_2$-brine-calcite systems as a function of pressure, temperature and salinity. The remainder of this manuscript is structured as follows. In Section 2, we provide a summary of the main features of the chosen force fields, the details of the system setup, and an overview of the simulation methodology implemented. In Section 3, we present the MD simulation results, starting from the assessment of the force fields, followed by the wettability studies. We summarize our concluding remarks in Section 4.

## 2. SIMULATON METHODS AND ALGORITHMS

### 2.1. Molecular models and force fields

The calcite slab was obtained from a calcite crystal terminated at the plane $[10\bar{1}4]$.[32] In the first instance, the calcite surface was modelled using the force field developed by Xiao et al.[33] This force field has been previously used to study the hydration layer structure near calcite surfaces as well as the calcium-mediated adhesion of nanomaterials to calcite.[34-35] In our implementation, calcium and carbon atoms were kept rigid, while the oxygen atoms were allowed to move. The force field proposed by Raiteri et al.[36] was also considered to describe calcite, for comparison purposes.

We implemented the elementary physical model with the intramolecular bond stretch and angle bend parameters developed by Cygan et al.[37] (EPM2) to describe $CO_2$. EPM2 is a flexible three-site model, which is able to describe accurately the interfacial behaviour and the vibrational state of $CO_2$ at supercritical conditions.[37] For simulations conducted by implementing the force field developed by Raiteri et al.[36] to describe calcite, we used the set of force field parameters proposed by Silvestri et al.[38] to describe the $CO_2$−calcite interactions. In this approach, the interactions between $CO_2$ and calcite were described by Buckingham and Coulomb potentials.

Although a number of different force field models are available for water, no single model accurately captures all its physical properties. To select the water model suitable for the present investigation, we conducted equilibrium MD simulations for a thin film of water supported on calcite. The following water models were compared: the simple point charge extended (SPC/E),[39] the simple point charge (SPC),[40] the SPC flexible (SPC-FW),[41] the

transferable intermolecular potential three-point model (TIP3P),[42] and the TIP four-point model in its 2005 derivation (TIP4P/2005).[43] Each model has advantages and disadvantages. The SPC/E model yields good results for structure and dynamics of bulk liquid water at ambient conditions[44-46] and for static dielectric constant over a very wide range of temperatures and densities,[47] but it underestimates water viscosity[48] and fails to reproduce experimental vapor pressure, as well as other thermodynamic properties at critical and supercritical conditions.[49] The SPC model is successful at reproducing the liquid-vapor coexistence curve and vapor pressure,[50-51] but it over-predicts the diffusion coefficient.[52] The SPC/Fw yields a better prediction of viscosity, diffusion coefficient, and dielectric constant at ambient conditions than SPC/E,[51-52] but it does not predict accurately isobaric heat capacity. The TIP4P/2005 model provides a good description of vapor–liquid equilibria densities,[53] surface tension,[54] and viscosity,[55] but it fails in reproducing simultaneously the vapor and the liquid phases of water,[53] as well as its dielectric constant.[56] The TIP3P model is commonly used to describe water interactions with biological molecules. However, it provides poor descriptions of water properties when compared to other models.[45, 56] A discussion is presented below that explains why the SPC/E water model was implemented to investigate the contact angle in calcite/brine/$CO_2$ systems as a function of T, P, and system composition.

The model proposed by Joung and Cheatham[57] was implemented for quantifying the properties of monovalent NaCl ions. This model yields reasonable estimates for the solubility of NaCl in water at room temperature (5.1 $mol_{NaCl}/kg_{H2O}$) when compared to experiments (6.15 $mol_{NaCl}/kg_{H2O}$).[58] In all simulations conducted here, the NaCl concentration was maintained below the solubility limit as predicted by the respective models.

In all simulations conducted by implementing the force field developed by Xiao et al.[33] to describe calcite, non-bonded dispersive interactions were modelled by the 12–6 Lennard–Jones (LJ) potential and electrostatics forces by implementing the Coulombic potential. The cut-off distance for interatomic interactions was fixed at 12 Å and the long-range electrostatic interactions were calculated using the particle-particle-particle-mesh (PPPM) solver.[59] The LJ parameters for all cross interactions between different atoms were determined by applying Lorentz−Berthelot mixing rules.[60]

### 2.2. Simulation Setup

The simulation box was periodic in the three directions for all simulations in this study and contained a slab of calcite supporting one thin film of fluid.

To validate the water models, we performed simulations with 4558 water molecules placed on the calcite surface, which yield a water film of ~ 30 Å in thickness. In these simulations, the x, y and z dimensions of the simulation box were 97.14, 90.0, and 158.9 Å, respectively. In our model, the solid substrate was placed with its surface parallel to the xy plane. Along the z direction, perpendicular to the solid surface, the box contained a slab of calcite of thickness 14.1 Å to provide the free-standing calcite support. The z direction of the simulation box is elongated because a layer of gas phase is allowed on top of the liquid film. Based on our prior work, this prevents boundary conditions to affect the results.

To study the wettability of calcite, we simulated systems in which a fluid droplet was placed on the substrate and it was then surrounded by the other fluid. Both water droplets surrounded by $CO_2$, and $CO_2$ droplets surrounded by water were simulated. To avoid line-tension effects, we simulated cylindrical droplets, placed on the box parallel to the x direction.[24,61] One initial configuration of the water droplet surrounded by $CO_2$ is shown in Figure 2. To generate the droplet, we first performed MD simulations of 2000 water molecules placed on calcite. The simulations were carried out in the NVT ensemble, with a box size 97.14 x 180 x 100 $Å^3$. In this set up, the y axis of the simulation box is elongated compared to the x axis. Because the cylindrical droplet is aligned parallel to the x axis, an elongated y axis prevents periodic boundary conditions from affecting the results. The final configuration of this simulation (Figure 2a) was then simulated in the presence of 10426 $CO_2$ molecules, as shown in Figure 2b. The subsequent simulations were conducted in the NPT ensemble, wherein the pressure was controlled perpendicular to the calcite surface. To study $CO_2$ droplets, we used a similar procedure, within a box of initial box size 97.14 x 180 x 110 $Å^3$. The z size of the simulation box was slightly increased compared to the prior simulations for computational reasons. As these simulations progressed, the length of the z axis of the box decreased to ~104 Å to maintain the desired pressure. We explored the behaviour of both pure water and NaCl brine at varying concentrations. The fluid phase compositions, as well as pressure, temperature and brine composition for each system simulated within the approach exemplified in Figure 2 are provided in Table 1.

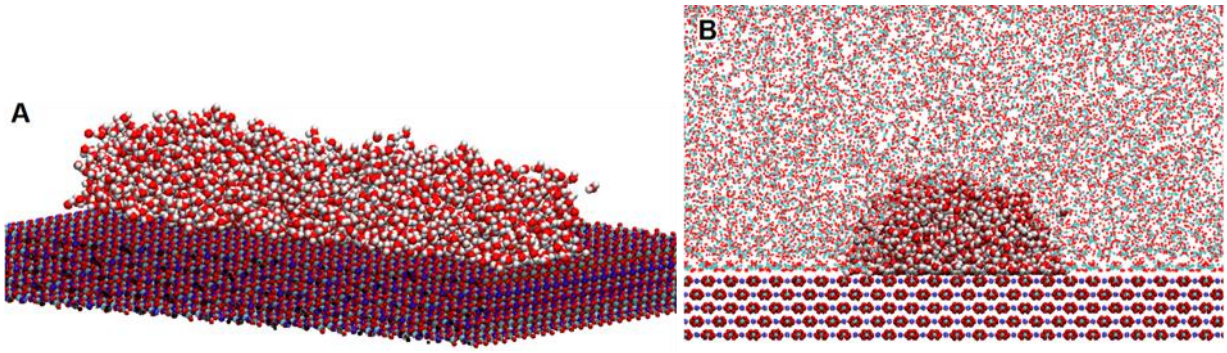


**Figure 2**. Initial configuration of one $H_2O$ droplet on the calcite surface (a) and in the presence of $CO_2$ (b). Ca = blue; C = cyan; O = red; H = white.

**Table 1**. Composition and thermodynamic conditions of the $CO_2$-brine-calcite systems simulated.

| | Number of molecules | | | Temperature (°C) | Pressure (MPa) |
|---|---|---|---|---|---|
| | $H_2O$ | $CO_2$ | NaCl | | |
| **$H_2O$ droplet in $CO_2$** | 2000 | 10426 | | 30 & 50 | 7 & 20 |
| 1.0 M NaCl droplet in $CO_2$ | 2000 | 10426 | 36 | 50 | 20 |
| 2.0 M NaCl droplet in $CO_2$ | 2000 | 10426 | 72 | 50 | 20 |
| 3.0 M NaCl droplet in $CO_2$ | 2000 | 10426 | 108 | 50 | 20 |
| **$CO_2$ droplet on $H_2O$** | 45000 | 2200 | | 50 | 20 |
| $CO_2$ droplet in 0.1 M NaCl | 45000 | 2200 | 81 | 50 | 20 |
| $CO_2$ droplet in 0.3 M NaCl | 45000 | 2200 | 243 | 50 | 20 |
| $CO_2$ droplet in 0.75 M NaCl | 45000 | 2200 | 608 | 50 | 20 |
| $CO_2$ droplet in 1.5 M NaCl | 45000 | 2200 | 1215 | 50 | 20 |

### 2.3. Algorithms

The assessment of water models was conducted by performing MD simulations using the package GROMACS (version 5.1.4)[62-63] in the canonical ensemble (NVT), where the number of particles (N), the simulation volume (V), and the temperature (T) are kept constant.
The equations of motion were integrated by implementing the leapfrog algorithm[64] with a time step of 1.0 fs. The temperature of calcite and that of the fluid phases were maintained constant at 298 K using two separate Nosé-Hoover thermostats.[65-66] This allowed us to maintain the correct kinetic energy distribution between solid and fluid.[67] Both thermostats had a relaxation time constant of 100 fs. The total simulation time for each system was 30 ns. The system was considered equilibrated when atomic water density profiles oscillated around a constant value, and both system energy temperatures fluctuated within 10% of their respective average values. Each simulation was repeated three times to assess the reliability of the results. The last 2 ns of the simulations were used for production and the simulated trajectories were used to extract the results presented in Section 3.1.

The simulations conducted to quantify the wettability of calcite were performed using the open-source LAMMPS code, version 20180818.[68] These simulations were carried out in the NPT ensemble (constant number of atoms, constant pressure, and constant temperature). The pressure was coupled in the z direction, perpendicular to the calcite surface, using the Nosé-Hoover barostat[69] with a relaxation time of 100 ps. The simulations were terminated when the droplet shape did not change and both fluids appeared stable within a simulated time of 12 ns. Each simulation was repeated three times to assess the reliability of the results.

### 2.4 Contact Angle Analysis

To identify the profile of a water droplet, the atomic density across the $CO_2$-water interface was fitted with the sigmoidal function:[70]

$$\rho(z) = \frac{1}{2}\rho_l\left[1 - \tanh\left(\frac{z - z_0}{d}\right)\right] \quad (2)$$

In Eq. (2), $\rho_l$ is the water liquid density, d is the width of the $CO_2$-water interface and $z_0$ is the position of the surface where the water density $\rho_0$ is halfway between the water bulk density and water density in the $CO_2$ phase.

Water contact angles were extracted from 2D density profiles obtained for the simulated water droplets fitted with Eq. (2). The iso-density contours at $\rho=\rho_0$ were used to determine the contact angle for all of the systems considered in this work. Once the droplet contours were known, a circular function was fit to them. Because density fluctuations occur near the calcite surface due to the water-calcite interactions, the region located within ~ 10 Å from the calcite surface was excluded from the fitting. The base of droplet was defined at the third hydration layer away from the calcite surface. The slopes of the tangent lines on both sides of droplet were averaged to extract the contact angle.

## 3. SIMULATION RESULTS

### 3.1. Assessment of Water Models

Among other phenomena that occur when a mineral surface is exposed to an aqueous solution, the formation of the hydration layer and its molecular structure are the most fundamental. Because the molecular structure within the hydration layer is of direct relevance to the wettability behaviour, the suitability of the water models for the present study is assessed based on their ability to replicate experimental atomic density profiles at the calcite–water interface. For these simulations, the calcite substrate was modeled by implementing the force field developed by Xiao et al.[33] In Figure 3, we present the atomic density profiles of O and H atoms of water as a function of the vertical distance from the calcite surface. The results provide evidence for the formation of two well-defined water layers near the surface when implementing each of the water models considered. In Table 2, we summarize the positions of the two hydration layers above the $[10\bar{1}4]$ calcite surface as predicted in this study, as well as results from earlier publications. The positions of the two hydration layers were determined by the distance between the calcium carbonate plane and that formed by water O atoms. Overall, the location of the first water layer in this study is in general agreement with previous experimental and MD simulation results. The five models implemented here to simulate water consistently predict the location of the first layer at 2.45 Å from the calcium atoms in the surface. This result is in agreement with the experimental X-ray scattering findings reported by Fenter et al.,[71] who found the presence of the oxygen atoms of water molecules at 2.50 ± 0.12 Å above the surface calcium ions. The five water models considered yield different positions for the second hydration layer. The result obtained from TIP3P model is in good agreement with the X-ray scattering experiments reported by Geissbühler et al.,[72] but results from SPC/E and SPC models are more consistent with X-ray reflectivity,[71] surface diffraction,[73] and surface X-ray scattering data.[72]

The simulation results for the density profiles of H atoms present more pronounced differences when different water models are implemented. It should be pointed out that the H

density profiles obtained when using either SPC or SPC/E water models are very similar. Of the models that yield results consistent with experiments, the SPC/E one was chosen for the present study because it is (a) computationally efficient, (b) reliable for assessing equilibrium structure and dynamics of liquid water, and (c) suitable for estimating the properties of aqueous electrolyte solutions. It should be pointed out that Nielsen et al.[74] found that the SPC/E model of water, when combined with the EPM2 model of $CO_2$, slightly overpredicts the water-$CO_2$ interfacial tension compared to experiments, and underpredicts the expected surface excess of $CO_2$. For completeness, it is worth pointing out that, in general, no combination of force fields based on the Lennard-Jones 12−6 functional form was found able to adequately represent properties of both coexisting phases of $CO_2$/$H_2O$ binary mixtures.[75-76] Using the EPM2−SPC/E combination, Vlcek et al.[77] optimized the cross term interaction parameters to accurately reproduce experimental mutual solubilities of water and $CO_2$ at supercritical $CO_2$ conditions. Orozco et al.[76] recently reported that the parameters optimised by Vlcek et al. yield excellent predictions for solubilities in the $H_2O$-rich phase, but not in the $CO_2$-rich one. These limitations were found not to be related to the cross-term parameters, but instead to the inherent limitations of the implemented model.[78]

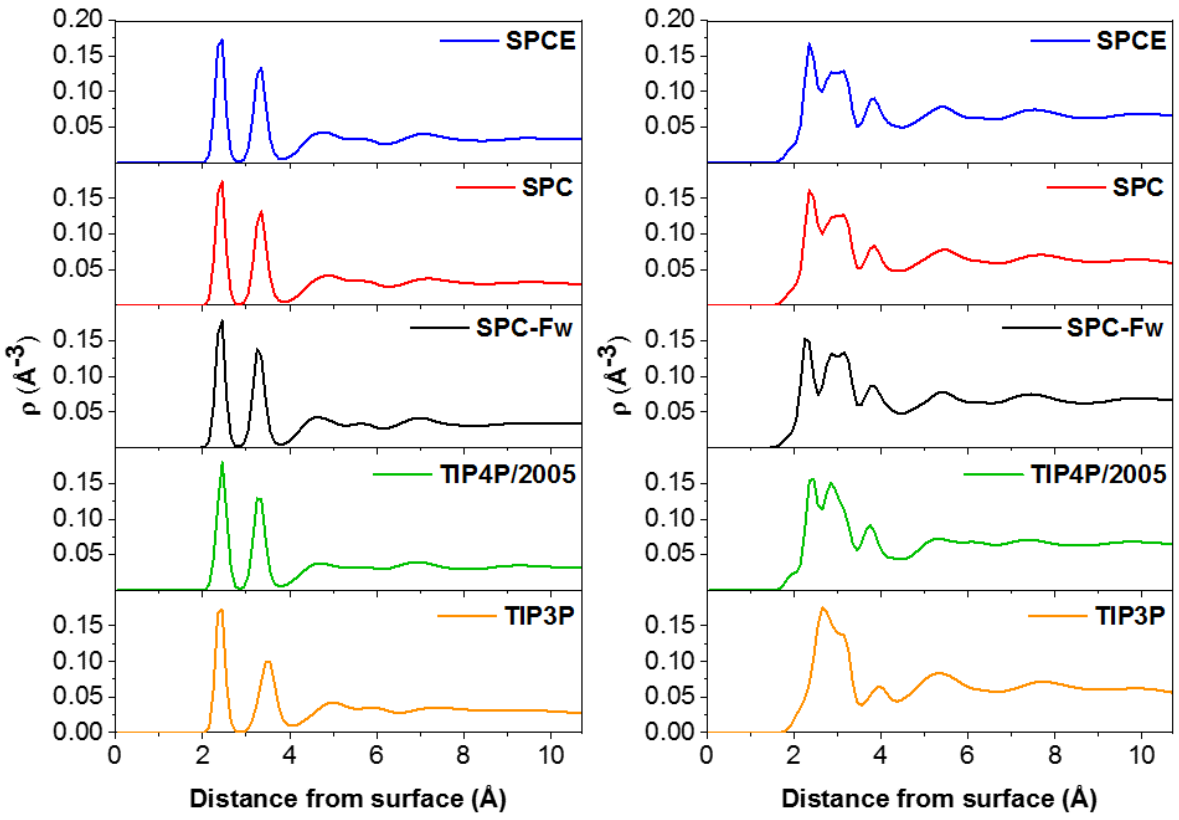


**Figure 3**. Atomic density profiles along the z direction, vertical from the surface, for the oxygen (A) and hydrogen (B) atoms of water molecules. The reference position (i.e., z = 0) is defined by the z-position of the plane of Ca atoms on the calcite surface. In these simulations, calcite is described by implementing the force field proposed by Xiao et al.[33]

**Table 2.** Comparison of water structure results obtained at the calcite surface.

| **Technique** | | **First layer (Å)** | **Second layer (Å)** |
|---|---|---|---|
| X-ray reflectivity[71] | | 2.50 ± 0.12 | – |
| X-ray reflectivity[79] | | 2.14 ± 0.02 | 3.44 ± 0.12 |
| Surface diffraction[73] | | 2.35 ± 0.10 | 3.24 ± 0.12 |
| Surface X-ray scattering[72] | | 2.3 ± 0.1 | 3.45 ± 0.2 |
| *Ab initio* simulation[80] | | 2.47 | – |
| Quantum MD[81] | | 2.4 | 3.2 |
| MD simulations from literature[82] | | 2.41 | 3.5 |
| MD simulations from literature[83] | | 2.43 | 3.63 |
| MD simulations (this work, Xiao et al.'s force field[33]) | SPC/E | 2.45 | 3.35 |
| | SPC | 2.45 | 3.35 |
| | SPC/Fw | 2.45 | 3.25 |
| | TIP4P/2005 | 2.45 | 3.25 |
| | TI3P | 2.45 | 3.45 |
| MD simulations (this work, Raiteri et al.'s force field[36]) | SPC/E | 2.19 | 3.31 |

### 3.2. Calcite Wettability

To quantify calcite wettability at conditions representative of GCS, water droplets surrounded by $CO_2$ were simulated on calcite at elevated P and T conditions. The chosen conditions represent shallow (30 °C and 7 MPa) and deep formations (50 °C and 50 MPa), representative of injection sites.[20] The amount of water in our simulations is intentionally much smaller than that of $CO_2$, in an attempt to replicate conditions near the well bore, where $CO_2$ is injected. Although as the simulations progress, $CO_2$ molecules dissolve within the water droplet, we did not attempt to quantify the $CO_2$ solubility as a function of, e.g., salt content in the aqueous phase.

To understand the contact angle dependency on salinity, we attempted to investigate NaCl brines at increasing concentration (1 M, 2 M and 3 M). Experimental results suggest that the water contact angle changes with temperature, pressure, and salinity. Our simulations, using the parameters of Xiao et al.[33] in combination with the SPC/E water model and the flexible version of the EPM2 model of Cygan et al.,[37] however, show that water and brine in the presence of $CO_2$ completely spread on calcite. This prevented us from estimating the contact angle using our approach. The evolution of the water and NaCl brine droplets supported on calcite as a function of simulation time is illustrated Figure 4a and c. Complete wetting was observed after ~ 24 ns of simulations. It seems that the simulation results are not consistent with reported macroscopic experimental observations due to the strong interactions between $H_2O$ and calcite. This could be because the force field implemented here to study calcite[33] was originally developed to mainly study the mechanical properties of $CaCO_3$, as well as the

interaction of $CaCO_3$ with water and proteins. To test this hypothesis, we conducted additional simulations implementing the force field developed by Raiteri et al.[36] to describe calcite and the set of force field parameters developed by Silvestri et al.[38] to model the interactions between $CO_2$ and calcite. Water is modeled with the SPC/E formalism in these simulations. We report in the Supporting Information (SI) details regarding these simulations. In Figure S2 of the SI, we report the density profiles of water obtained implementing both the force field parameters developed by Xiao et al.[33] and those by Raiteri et al.[36] In the SI we also display the simulation results reported by Reischl et al.[83] The distances between the water oxygen atoms in the first, second, and third water layers predicted by our simulations conducted implementing the force field developed by Raiteri et al.[36] are ~ 2.19, 3.31, and 4.81 Å, respectively, from the calcium carbonate plane on the calcite substrate. The first and second of these values are at shorter distances compared to those predicted when the force field developed by Xiao et al.[33] was implemented (i.e., see Table 2). However, they agree reasonably well with experimental results from surface X-ray scattering[72] and surface diffraction,[73] respectively. The positions of the three hydration layers as reported by Reischl et al.[83] are 2.43, 3.63, and 4.91 Å, respectively which are also in good agreement with the experimental data shown in Table 2. Our analysis suggests that the force field developed by Raiteri et al.[36] yields an interfacial water structure that is similar to the one predicted by implementing the force field proposed by Xiao et al.[33]; while there are some differences, in general both sets of predictions are in reasonable agreement with available experiments.

We therefore used the force field parameters proposed by Raiteri et al.[36] and Silvestri et al.[38] in combination with the SPC/E water model to predict the contact angle. To quantify the effect of droplet size on the predicted contact angle, a series of simulations were conducted using water droplets of different initial radii. Details for the simulated systems are summarized in Table S1 of the SI. Figure 4c shows one of the final configurations of one water droplet without salt simulated on the calcite surface in the presence of $CO_2$. The corresponding 2D density profile and tangent lines for contact angle prediction are presented in Figures S3 and S4 of the SI. The contact angle for $CO_2$-saturated water droplet on the calcite surface in the presence of $CO_2$ at 50° C and 20 MPa is found to converge to ~ 46° as the droplet size increases (see Figure S5 in the SI). By comparison, Silvestri et al.[31] recently reported water contact angles on calcite of 38° at 50° C and 20 MPa. Our simulation results strongly deviate from the experimental data reported by Arif et al.,[28] who measured advancing ($\theta_a$) and receding ($\theta_r$) contact angles for $CO_2$/water/calcite systems and found that $\theta_a$ ~ 90° and $\theta_r$ ~ 80°. However, our simulations are somewhat consistent with the experimental data reported by Wang et al.,[20] who reported the contact angle for water on calcite of ~ 26.2° at 50° C and 20 MPa.

Our analysis suggests that the force field parameters developed by Raiteri et al.[36] and Silvestri et al.[38] should be reliable for the prediction of the water contact angle for $CO_2$/water/calcite systems. However, because the force field developed by Xiao et al.[33] provides water density profiles near the calcite substrate that are in very good agreement with available experiments, as discussed in Section 3.1, and because some experimental data report very different values for the contact angle, as discussed above, it remains possible that

the sources for the discrepancy between simulated and experimental contact angles are due to other effects, including the possibility that experimental calcite substrates are not perfect single crystal structures such as those simulated here. Further studies are required to clarify this situation and to test whether impurities such as organics might affect the contact angles. It should be pointed out that the force field parameters proposed by Silvestri et al.[38] has not yet been extended to include interactions with salt ions.

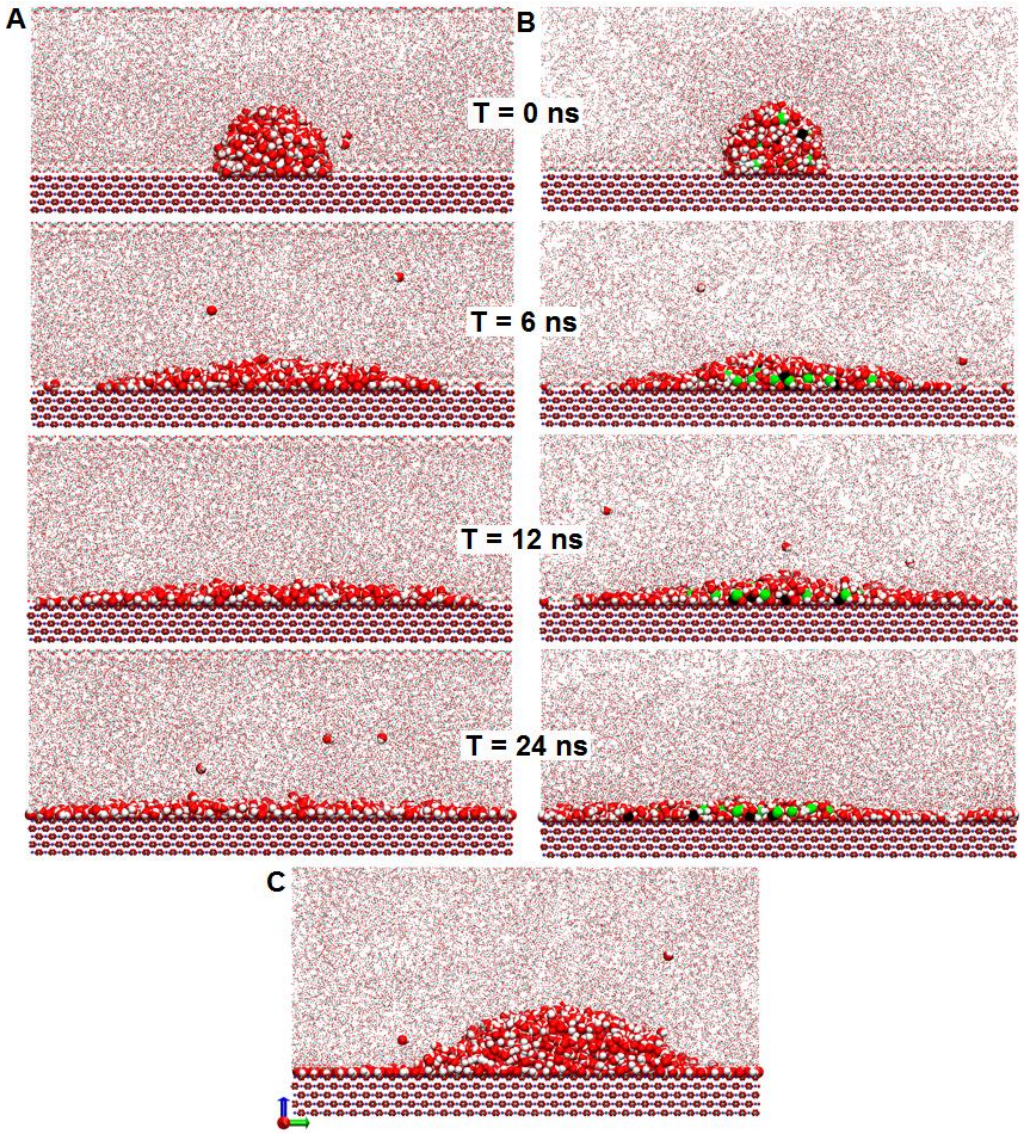


**Figure 4.** Sequence of simulation snapshots for (A) one water droplet containing no salt, and (B) one water droplet containing 3 M NaCl salt as a function of simulation time. These simulations are conducted with the force field proposed by Xiao et al.[33] to describe calcite. (C) Snapshot of one pure water droplet after equilibration from simulations conducted by implementing the force field proposed by Raiteri et al.[36] to describe calcite and the set of force field parameters proposed by Silvestri et al.[38] to describe the $CO_2$–calcite interactions. These results were obtained simulating 5000 $H_2O$ molecules in the presence of 10426 $CO_2$ molecules. All droplets are simulated in the presence of $CO_2$. The simulations were conducted at 50 °C and 20 MPa. Ca = blue; C = cyan; O = red; H = white, $Na^+$ = black; and $Cl^-$ = green.

Even though injected supercritical $CO_2$ is typically the non-wetting phase in the presence of brine in many sedimentary rocks, it is of interest to quantify how $CO_2$ behaves on wet surfaces. For example, Wang et al.[29] investigated experimentally the adhesion of $CO_2$ on several homogeneous mineral surfaces, including calcite, under reservoir P and T conditions (50°C and 20 MPa). They reported that the addition of salt increased significantly $CO_2$ adhesion. The relationship between wettability, adhesion, and water layer structure was studied by Buckley et al.[84] They suggested that the wettability of the mineral surface could be altered by introducing acids/bases to the system to break the electrical double layer structure and provide a strong charge imbalance at the surface. Liu et al.[81] performed extensive quantum MD simulations to investigate the mechanisms responsible for wettability alteration of calcite. Density profiles of water and NaCl salt ions normal to the surface were calculated, as well as those of other ions such as $Ca^{2+}$, $Mg^{2+}$ and $SO_4^{2-}$. They found that $Na^+$ and $Cl^-$ ions render the surface less water-wet, while $Ca^{2+}$, $Mg^{2+}$ and $SO_4^{2-}$ render the surface more water-wet. To complement these simulations and in an attempt to connect to experiments, we assessed the affinity between $CO_2$ droplets and calcite in the presence of an aqueous-rich phase of various compositions (see Table 1). Although the force field parameters developed by Raiteri et al.[36] and Silvestri et al.[38] yield water contact angles on calcite, in the presence of $CO_2$, which are in accordance with some experiments, those force fields do not yet allow for the inclusion of salt ions. For completeness, we conducted simulations for $CO_2$ droplets surrounded by pure water near calcite implementing the force field parameters developed by Raiteri et al.[36] and Silvestri et al.[38] in combination with the SPC/E water model. The results (Figure 5) show that the $CO_2$ droplet remains very close to the second hydration layer on calcite, which is consistent with the observations reported by Silvestri et al.,[38] suggesting that strong interactions are present between $CO_2$ and the hydration water on calcite. The effect of NaCl brine concentrations on $CO_2$ droplet implementing the force fields developed by Raiteri et al.[36] and Silvestri et al.[38] were not considered in this study.

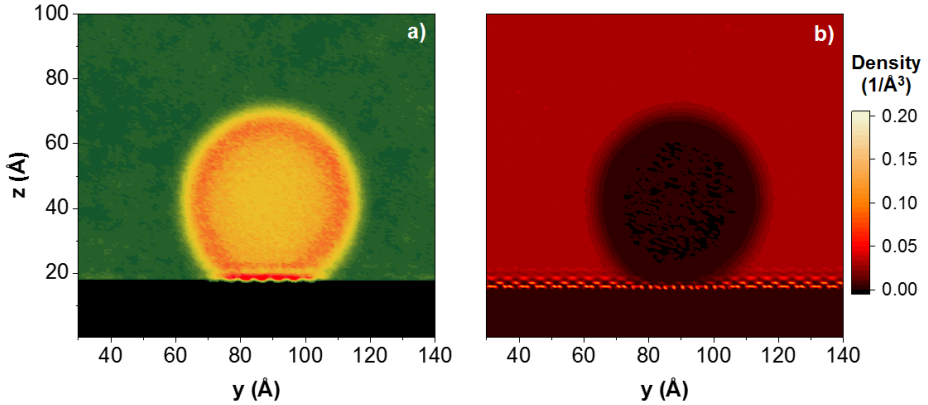


**Figure 5.** 2D density profiles of the $CO_2$ and $H_2O$ averaged over the 2 ns of production run. The $CO_2$ droplet was surrounded by pure water. The simulations were conducted at 50 °C and 20 MPa. Results are obtained for a) $CO_2$ and b) $H_2O$. The color bar expresses density in the units of $1/Å^3$. These simulations are conducted with the force field proposed by Raiteri et al.[36] to describe calcite and the set of force field parameters proposed by Silvestri et al.[38] to describe the $CO_2$–calcite interaction.

Because our results, combined with experimental data from literature, do not conclusively rule out that the force field proposed by Xiao et al.[33] yields reliable results, and because this force field allows us to investigate the effect of NaCl concentration, we used this force field to quantify the effect of NaCl concentration. The resultant snapshots for the final configurations of cylindrical $CO_2$ droplets near calcite in the presence of different NaCl brines are shown in Figure 6. To complement and better quantify the results from simulation snapshots shown in Figure 6, we calculated 2D density profiles of $CO_2$ and the surrounding fluids at various conditions within the plane perpendicular to the axis of the cylindrical droplet. For example, in Figure 7, we display the 2D density profiles of $CO_2$ and $H_2O$ when the $CO_2$ droplet was surrounded by pure water at 50 °C and 20 MPa. It can be seen that the $CO_2$ droplet did not adhere to calcite, possibly because of the extremely low contact angle predicted for water on calcite by our simulations, as displayed in Figure 4a and b.

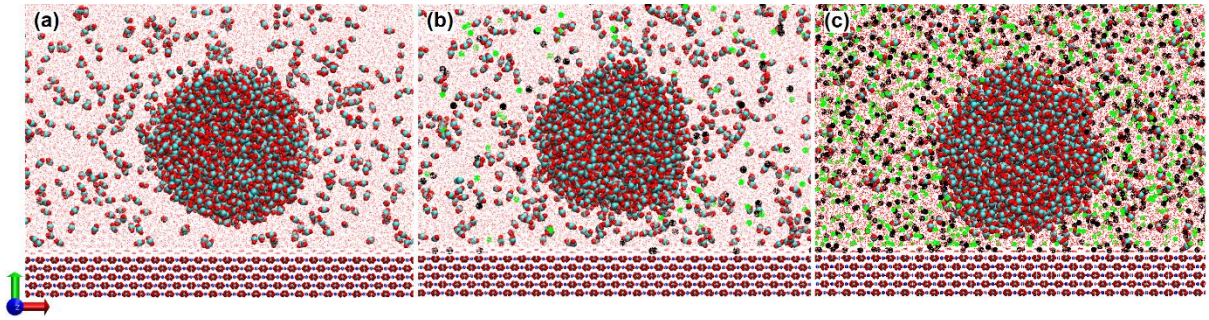


**Figure 6.** Snapshots of $CO_2$ droplets on the calcite surface in the presence of (a) pure water, 0.1 M NaCl brine and (c) 0.15 M NaCl brine. Small red dots represent $H_2O$ molecules, and cyan, black, and green spheres represent carbon atoms, $Na^+$ and $Cl^-$ ions, respectively. These simulations are conducted with the force field proposed by Xiao et al.[33] to describe calcite.

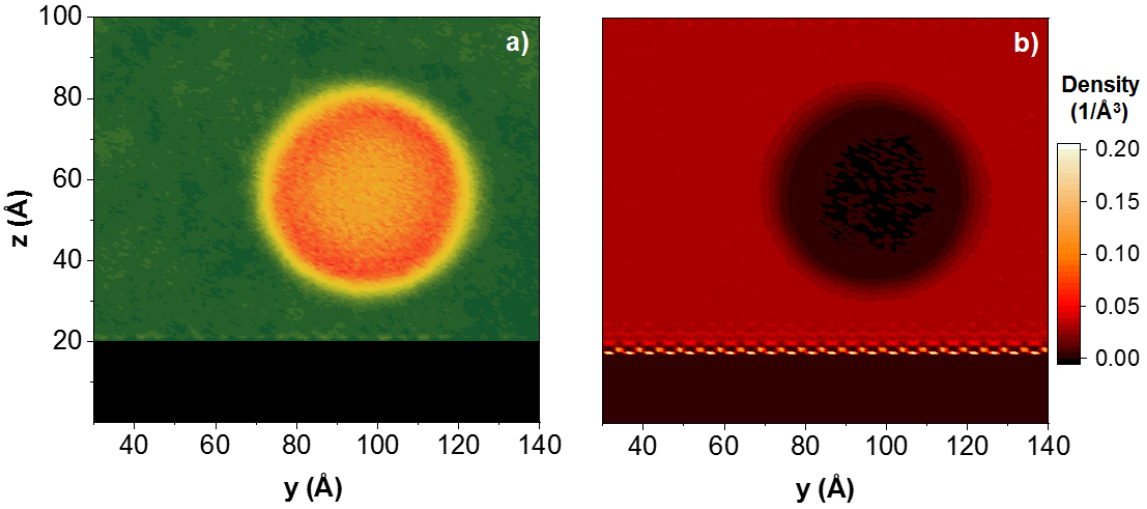


**Figure 7**. 2D density profiles of the $CO_2$ and $H_2O$ averaged over the 2 ns of production run. The $CO_2$ droplet was surrounded by pure water. The simulations were conducted at 50 °C and 20 MPa. Results are obtained for a) $CO_2$ and b) $H_2O$. The color bar expresses density in the units of $1/Å^3$. These simulations are conducted with the force field proposed by Xiao et al.[33] to describe calcite.

The observations from Figure 7 can be compared to similar ones obtained as the brine composition changes. In Figure 8, we report the 2D density profiles for $CO_2$ droplets near calcite in the presence of different NaCl brine concentrations. Although the $CO_2$ droplets did not adhere to the calcite surface, as NaCl concentration increases from 0.1 M to 1.5 M, the $CO_2$ droplet seems to become more affine to calcite with a slight tendency to approach the surface. This suggests that as NaCl concentration increases, the calcite surface becomes less water-wet, potentially because the salt ions affect the interfacial hydrogen bond network. This is consistent with the results reported by Liu et al.,[81] who suggested that the calcite surface becomes less water-wet due to the weak adhesion between the surface and NaCl brine. Liu et al.[81] reported that the calcite surface becomes oil-wet in the presence of 0.6 M NaCl brine.
The results in Figures 8 demonstrate that salinity plays an important role in controlling the interactions between $CO_2$ droplets and calcite surfaces. In Figures 9, we also report the 2D densities of $H_2O$ within the plane perpendicular to the axis of the cylindrical $CO_2$ droplet. The results show clearly that adding salt brings the $CO_2$ droplet closer to the calcite surface. In the remainder of this section we attempt to use simulation results to identify the driving forces for the results just summarised.

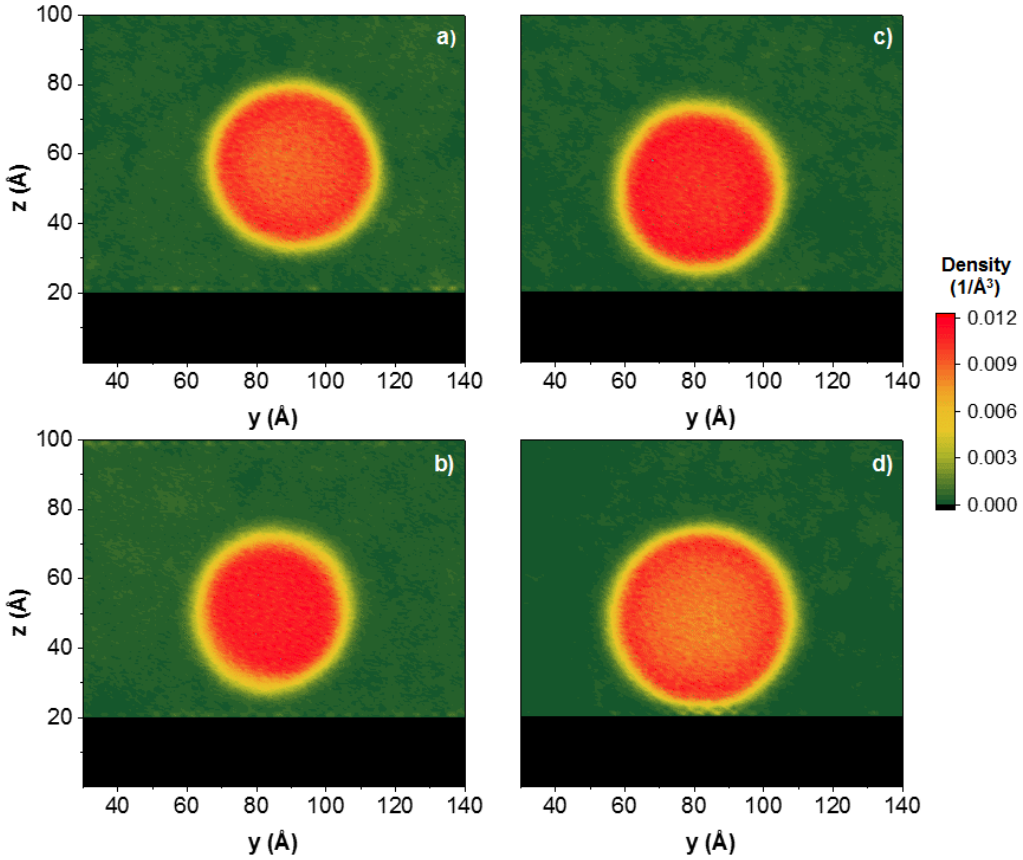


**Figure 8**. 2D density profiles of $CO_2$ droplets near calcite in the presence of NaCl brine at increasing salt concentration: (a) 0.1 M, (b) 0.3 M, (c) 0.75 M, and (d) 1.5 M. The simulations are conducted at 50 °C and 20 MPa and the last 2 ns of the simulations are used for data analysis. The color bar expresses density in the unit of $1/Å^3$. These simulations are conducted with the force field proposed by Xiao et al.[33] to describe calcite.

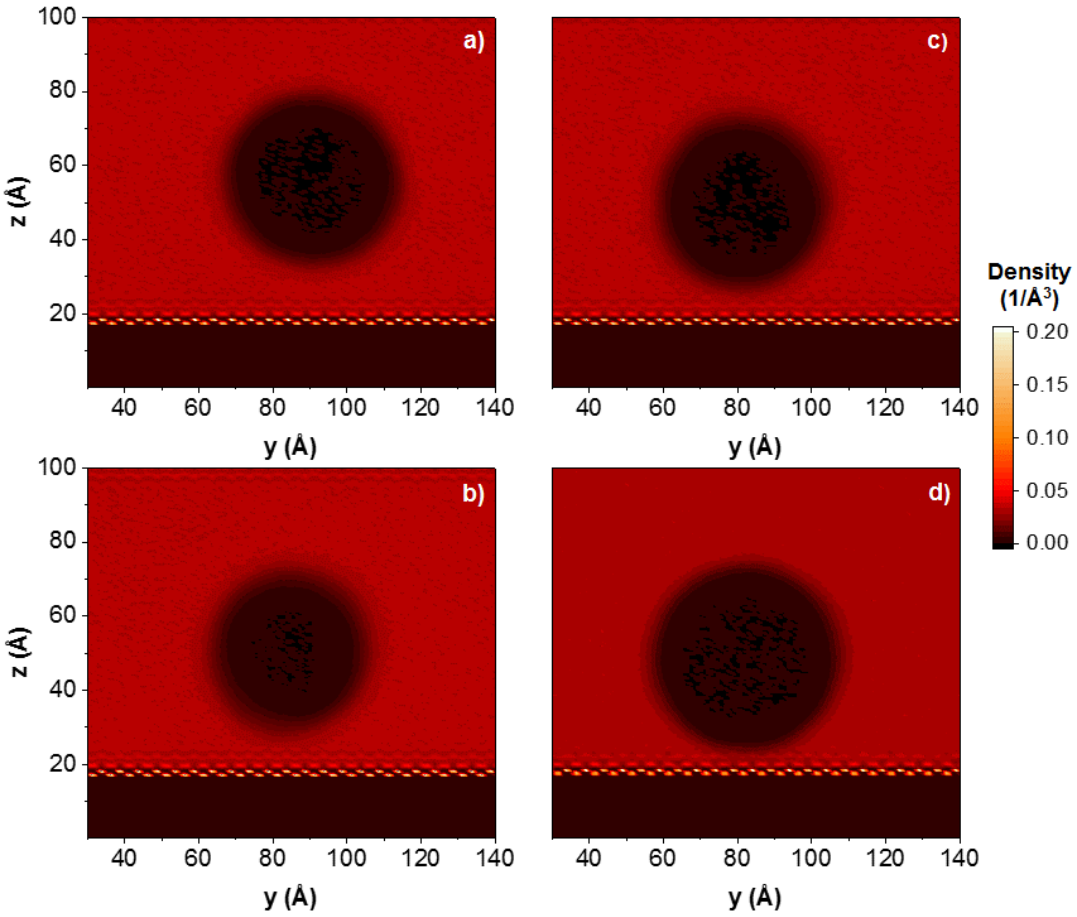


**Figure 9**. 2D density distributions of water oxygen atoms averaged over the final 2 ns of simulation conducted at 50 °C and 20 MPa on the calcite surface in the presence of NaCl brine at increasing salt concentration (a) 0.1 M, (b) 0.3 M, (c) 0.75 M, and (d) 1.5 M. The color bar expresses density in the unit of 1/Å$^3$. These simulations are conducted with the force field proposed by Xiao et al.[33] to describe calcite.

In Figure 10, we show the density profiles of water and NaCl salt ions normal to the surface. The results show that water molecules formed two layers strongly adsorbed to the calcite surface, consistent with the results shown in Figure 3. The hydration layers affect the ability of the NaCl ions to directly interact with calcite.

The ions density distributions reveal that $Na^+$ ions prefer to accumulate closer to the surface when compared to the $Cl^-$ anions. $Na^+$ ions exhibit one pronounced density peak centered at ~3.00 Å, which is in between the O density peaks representative of the first and second hydration layers. In contrast, the $Cl^-$ ions occur as two density peaks at ~ 5.00 and 7.35 Å. The height of the first $Na^+$ peak indicates that these ions strongly adsorb near the calcite/brine interface. This is supported by the planar density distributions obtained for the ions in the plane perpendicular to the droplet, shown in Figure 11. These results suggest the highest density of $Na^+$ ions is co-located with the first adsorbed layer on calcite, consistent with the results in Figure 10. Similarly, the $Cl^-$ density is highest within the surface hydration region, above the positive Stern layer formed by $Na^+$ ions on the first water monolayer at the surface.[85] It should be noted that these results are in contrast with those obtained from

aqueous NaCl solutions simulated on a model silica crystalline surface.[86-87] When the surface non-bridging oxygen atoms were fully protonated, $Cl^-$ ions were found to preferentially adsorb closer to the model silica surface than $Na^+$ ones. Both the structure of interfacial water and the availability of surface sites on which the ions can preferentially adsorb are responsible for these differences.

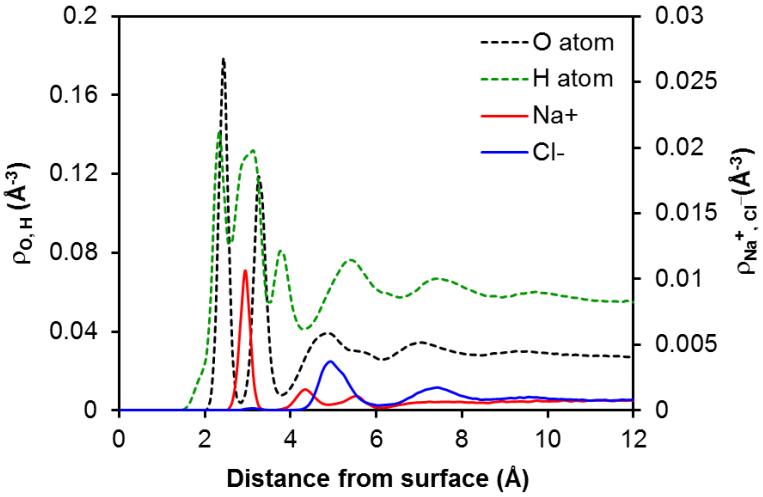


**Figure 10.** Z-density profiles of water and NaCl salt ions along the surface normal. The $CO_2$ droplet was surrounded by 1.5 M NaCl brine. The results were averaged over the last 2 ns of simulations conducted at 50 °C and 20 MPa. The location of the calcite surface (at z = 0) is defined by the position of the plane of the surface Ca atoms. The results for other concentrations are shown in the SI. These simulations are conducted with the force field proposed by Xiao et al.[33] to describe calcite.

To further investigate the effects of NaCl on the interfacial properties of the system, we examined the surface density distribution of water oxygen atoms within the first two hydration layers and how they are affected by the presence of NaCl ions. The hydration layers are identified from the position of the O density peaks in Figure 10. In Figure 12, we provide the surface density distribution of oxygen atoms within the first hydration layer, located at 2.9 Å from the plane of surface Ca atoms, and oxygen atoms within the second hydration layer, located 1 Å further from the first layer. The oxygen atoms in the first hydration layer yield a well-organized structure. It is likely that the pronounced structure of the first hydration layer is responsible for both the extremely low contact angle observed for water in our simulations (see Figure 4a and b) and also for not allowing the $CO_2$ droplets to adhere directly on the surface. Density distributions at different salt content are shown in the SI.

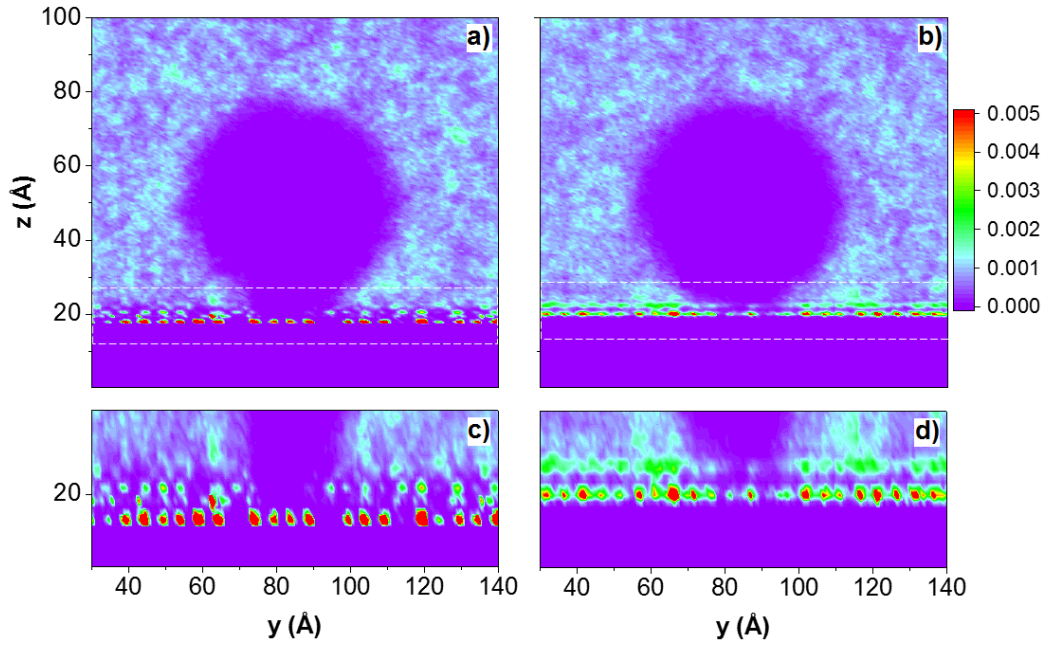


**Figure 11**. 2D density profiles of (a) $Na^+$ and (b) $Cl^-$ ions surrounding the $CO_2$ droplet. The $CO_2$ droplet was surrounded by 1.5 M NaCl brine. The simulations are conducted at 50 °C and 20 MPa and the last 2 ns of the simulations are used for data analysis. Note the accumulation of ions, in particular $Na^+$, near the calcite substrate. The color bar expresses density in the unit of $1/Å^3$. In panels (c) and (d) we report expanded views of the interfacial region from panels (a) and (b), respectively. These simulations are conducted with the force field proposed by Xiao et al.[33] to describe calcite.

The oxygen density distributions in the second hydration layer, shown in the bottom panels of Figure 12, show that NaCl ions strongly disrupts the arrangement of water molecules, as demonstrated by the missing accumulation of oxygen atoms within the regions highlighted by circles in panels (c) and (d). To complete the structural analysis of water molecules on the calcite surface, we also investigated the surface density distribution of hydrogen atoms within two hydration layers. These results are reported in the SI. In general, NaCl salt ions affect the distribution of hydrogen atoms in both hydration layers, which suggests that the interfacial water structure is modified.

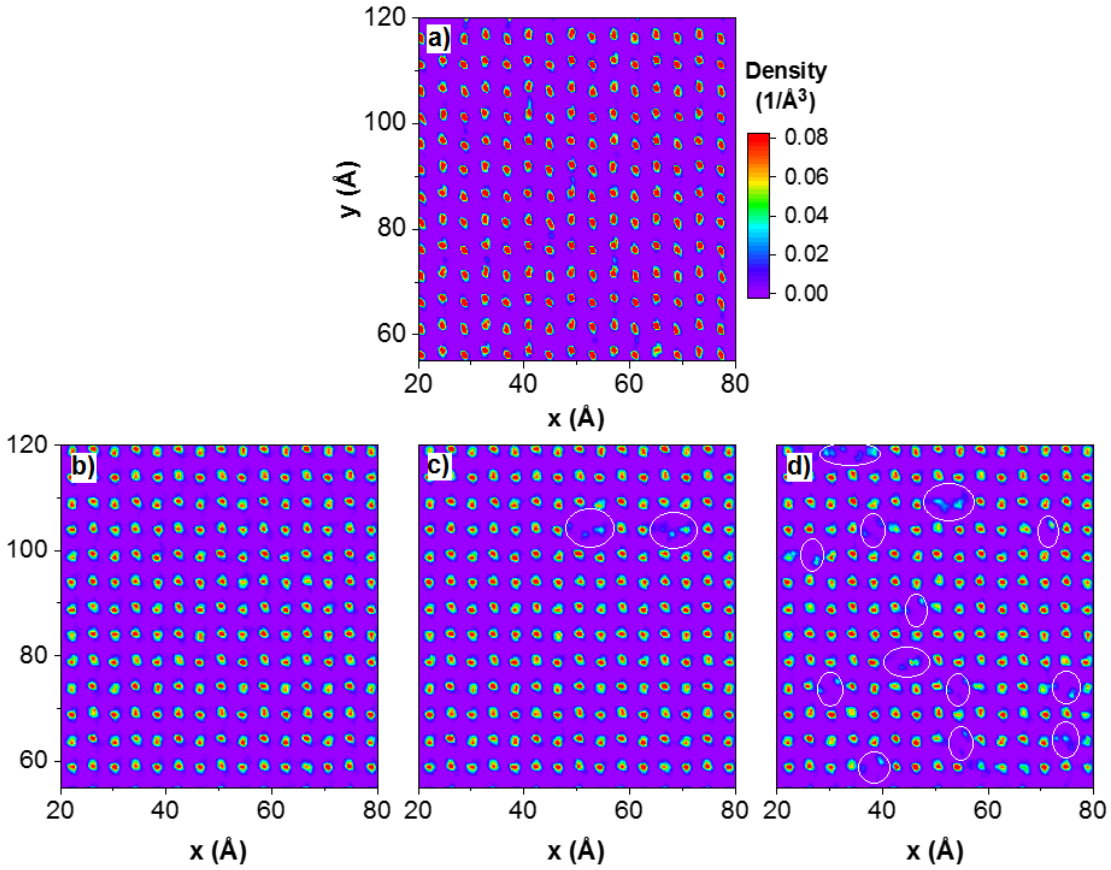


**Figure 12**. Surface density distribution of oxygen atoms within (a) the first and (b-d) the second hydration layer parallel to the X–Y plane. The figure shows result of the first hydration layer obtained for the system in which the $CO_2$ droplet was surrounded by 1.5 M NaCl brine. Because the surface density distribution of oxygen atoms within the first hydration layer is similar for all systems, only one representative is shown for brevity in panel (a). The results of the second hydration layer were obtained for systems in which $CO_2$ droplet surrounded by pure water (b) and by NaCl brine at increasing salt concentration: (c) 0.1 M, and (d) 1.5 M. The results for other concentrations are shown in the SI. The color bar expresses density in the unit of $1/Å^3$. These simulations are conducted with the force field proposed by Xiao et al.[33] to describe calcite.

## 4. CONCLUSIONS

The wettability of the calcite surface was probed using atomistic molecular dynamics simulations. Two force fields were compared to model the solid substrate, and several to model water. In general, the models reproduced reasonably well the structure of the first two hydration layers of water formed on calcite as observed experimentally. However, when the force fields parameterisation proposed by Xiao et al.[33] was implemented, the strong water-wetting behaviour predicted for the calcite surface prevented direct observation of the water contact angle as a function of temperature, pressure and salinity. In fact, within the limits of our simulations, complete wetting of the calcite surface by pure water or NaCl brine solutions was observed, which seems at odds with available experimental data. When the simulations

are conducted for one aqueous super-critical $CO_2$ droplet near calcite, the results strongly suggest that brine composition alters the affinity between a $CO_2$ droplet and calcite. In particular, NaCl ions disturb the hydration layers on calcite, which directly affects the affinity between the $CO_2$ droplet and the wet calcite surface. The simulation results suggest that increasing NaCl salt concentration allows the supercritical $CO_2$ droplet to more closely approach the surface.

When the force fields proposed by Raiteri et al.[36] and Silvestri et al.[38] were implemented to model calcite, the simulation results showed a contact angle for pure water, surrounded by $CO_2$, of ~ 46º. This value is in partial agreement with some experimental data, as reported in the literature, but others report contact angles as high as 80-90º. The set of force field parameters proposed by Silvestri et al.[38] has not yet been extended to investigate NaCl, and therefore we could not quantify the effect of salt content on wetting properties. When a super-critical $CO_2$ droplet was simulated near calcite in the presence of pure water, the simulation results suggested strong adhesion between the $CO_2$ droplet and the second hydration layer on calcite.

These results strongly suggest that force fields need to be improved to quantitatively capture the wetting properties of brine-$CO_2$-calcite systems via atomistic molecular simulations. However, the results suggest that ions dissolved in water can have a strong effect on the wetting properties. Further studies are required to fully quantify the effect of salt type and concentration, as well as the effect of impurities. Once these effects are quantified, a better understanding of the important role played by brines in controlling the $CO_2$ wettability of caprocks is expected, which will yield more reliable predictions concerning structural trapping capacity and containment security in geological carbon sequestration.

**Supplementary Information**

Density profiles of NaCl salt ions along the Z direction, water density profiles, composition of simulated systems, determination of $CO_2$-water interface, water contact angle prediction, water contact angle as a function of initial droplet radius, surface density distribution of oxygen atoms within the first and second hydration layer, surface density distribution of hydrogen atoms within the first and second hydration layer.

**Acknowledgments.** We acknowledge the financial support from the U.S. Department of Energy, Office of Basic Energy Sciences, under Contract No. DE-SC0006878 (Division of Chemical Sciences, Geosciences, and Biosciences), Geosciences Program. Additional financial support was provided by the A. P. Sloan Foundation via the Deep Carbon Observatory administered by the Carnegie Institution for Science. AS acknowledges financial support from the Science4CleanEnergy consortium (S4CE), which is supported by the Horizon2020 R&D programme of the European Commission, via grant No. 764810. Generous allocations of computing time were provided by the National Energy Research Scientific Computing Center (NERSC) at Lawrence Berkeley National Laboratory, Berkeley, CA. NERSC is supported by the DOE Office of Science. We are also grateful to the University College London Research Computing Platforms Support (MYRAID and GRACE) and the UK Materials and Molecular Modelling Hub (THOMAS), for access to high-performance computing.

## REFERENCES


1. White, C. M.; Strazisar, B. R.; Granite, E. J.; Hoffman, J. S.; Pennline, H. W., Separation and Capture of $CO_2$ from Large Stationary Sources and Sequestration in Geological Formations–Coalbeds and Deep Saline Aquifers. *J. Air Waste Manag. Assoc.* **2003**, *53*, 645-715.
2. Celia, M. A.; Bachu, S.; Nordbotten, J. M.; Bandilla, K. W., Status of $CO_2$ Storage in Deep Saline Aquifers with Emphasis on Modeling Approaches and Practical Simulations. *Water Resour. Res.* **2015**, *51*, 6846-6892.
3. Bruant, R. G.; Jr, Jr.; Celia, M. A.; Guswa, A. J.; Peters, C. A., Peer Reviewed: Safe Storage of $CO_2$ in Deep Saline Aquifiers. *Environ. Sci. Technol.* **2002**, *36*, 240A-245A.
4. Oldenburg, C. M.; Lewicki, J. L., On Leakage and Seepage of $CO_2$ from Geologic Storage Sites into Surface Water. *Environ. Geol.* **2006**, *50*, 691-705.
5. Doughty, C., Investigation of $CO_2$ Plume Behavior for a Large-Scale Pilot Test of Geologic Carbon Storage in a Saline Formation. *Transp Porous Med.* **2010**, *82*, 49-76.
6. Iglauer, S.; Pentland, C. H.; Busch, A., $CO_2$ Wettability of Seal and Reservoir Rocks and the Implications for Carbon Geo-Sequestration. *Water Resour. Res.* **2015**, *51*, 729-774.
7. Hesse, M. A.; Orr, F. M.; Tchelepi, H. A., Gravity Currents with Residual Trapping. *J. Fluid Mech.* **2008**, *611*, 35-60.
8. Iglauer, S. Dissolution Trapping of Carbon Dioxide in Reservoir Formation Brine–A Carbon Storage Mechanism. In *Mass Transfer-Advanced Aspects*; Nakajima, H., Ed.; Rijeka, Croatia: InT ech, 2011; pp 233-262.
9. Gaus, I., Role and Impact of $CO_2$–Rock Interactions During $CO_2$ Storage in Sedimentary Rocks. *Int. J. Greenh. Gas Control.* **2010**, *4*, 73-89.
10. Iglauer, S.; Al-Yaseri, A. Z.; Rezaee, R.; Lebedev, M., $CO_2$ Wettability of Caprocks: Implications for Structural Storage Capacity and Containment Security. *Geophys. Res. Lett.* **2015**, *42*, 9279-9284.
11. Krevor, S.; Blunt, M. J.; Benson, S. M.; Pentland, C. H.; Reynolds, C.; Al-Menhali, A.; Niu, B., Capillary Trapping for Geologic Carbon Dioxide Storage – From Pore Scale Physics to Field Scale Implications. *Int. J. Greenh. Gas Control.* **2015**, *40*, 221-237.
12. Al-Menhali, A. S.; Krevor, S., Pore-Scale Analysis of in Situ Contact Angle Measurements in Mixed-Wet Rocks: Applications to Carbon Utilization in Oil Fields. *Energy Procedia* **2017**, *114*, 6919-6927.
13. Iglauer, S.; Fernø, M. A.; Shearing, P.; Blunt, M. J., Comparison of Residual Oil Cluster Size Distribution, Morphology and Saturation in Oil-Wet and Water-Wet Sandstone. *J. Colloid Interface Sci.* **2012**, *375*, 187-192.
14. Tokunaga, T. K.; Wan, J., Capillary Pressure and Mineral Wettability Influences on Reservoir $CO_2$ Capacity. *Rev. Mineral. Geochem.* **2013**, *77*, 481-503.
15. Young, T., An Essay on the Cohesion of Fluids. *Philosophical Transactions of the Royal Society of London* **1805**, *95*, 65-87.
16. Adamson, A. W.; Gast, A. P., *Physical Chemistry of Surfaces*; Wiley-Interscience, N.Y., 1997.
17. Dickson, J. L.; Gupta, G.; Horozov, T. S.; Binks, B. P.; Johnston, K. P., Wetting Phenomena at the $CO_2$/Water/Glass Interface. *Langmuir* **2006**, *22*, 2161-2170.
18. Espinoza, D. N.; Santamarina, J. C., Water-$CO_2$-Mineral Systems: Interfacial Tension, Contact Angle, and Diffusion–Implications to $CO_2$ Geological Storage. *Water Resour. Res.* **2010**, *46*, W07537.
19. Bikkina, P. K., Contact Angle Measurements of $CO_2$–Water–Quartz/Calcite Systems in the Perspective of Carbon Sequestration. *Int. J. Greenh. Gas Control.* **2011**, *5*, 1259-1271.

20. Wang, S.; Edwards, I. M.; Clarens, A. F., Wettability Phenomena at the $CO_2$–Brine–Mineral Interface: Implications for Geologic Carbon Sequestration. *Environ. Sci. Technol.* **2013**, *47*, 234-241.
21. Iglauer, S., $CO_2$–Water–Rock Wettability: Variability, Influencing Factors, and Implications for $CO_2$ Geostorage. *Acc. Chem. Res.* **2017**, *50*, 1134-1142.
22. Chen, C.; Dong, B.; Zhang, N.; Li, W.; Song, Y., Pressure and Temperature Dependence of Contact Angles for $CO_2$/Water/Silica Systems Predicted by Molecular Dynamics Simulations. *Energy Fuels* **2016**, *30*, 5027-5034.
23. Iglauer, S.; Mathew, M. S.; Bresme, F., Molecular Dynamics Computations of Brine–$CO_2$ Interfacial Tensions and Brine–$CO_2$–Quartz Contact Angles and Their Effects on Structural and Residual Trapping Mechanisms in Carbon Geo-Sequestration. *J. Colloid Interface Sci.* **2012**, *386*, 405-414.
24. Tenney, C. M.; Cygan, R. T., Molecular Simulation of Carbon Dioxide, Brine, and Clay Mineral Interactions and Determination of Contact Angles. *Environ. Sci. Technol.* **2014**, *48*, 2035-2042.
25. Arif, M.; Abu-Khamsin, S. A.; Iglauer, S., Wettability of Rock/$CO_2$/Brine and Rock/Oil/$CO_2$-Enriched-Brine Systems: Critical Parametric Analysis and Future Outlook. *Adv. Colloid Interface Sci*. **2019**, *268*, 91-113.
26. Jafari, M.; Jung, J., Direct Measurement of Static and Dynamic Contact Angles Using a Random Micromodel Considering Geological $CO_2$ Sequestration. *Sustainability* **2017**, *9*, 2352.
27. Chen, C.; Wan, J.; Li, W.; Song, Y., Water Contact Angles on Quartz Surfaces under Supercritical $CO_2$ Sequestration Conditions: Experimental and Molecular Dynamics Simulation Studies. *Int. J. Greenh. Gas Control.* **2015**, *42*, 655-665.
28. Arif, M.; Lebedev, M.; Barifcani, A.; Iglauer, S., $CO_2$ Storage in Carbonates: Wettability of Calcite. *Int. J. Greenh. Gas Control.* **2017**, *62*, 113-121.
29. Wang, S.; Tao, Z.; Persily, S. M.; Clarens, A. F., $CO_2$ Adhesion on Hydrated Mineral Surfaces. *Environ. Sci. Technol.* **2013**, *47*, 11858-11865.
30. Abdallah, W.; Gmira, A., Wettability Assessment and Surface Compositional Analysis of Aged Calcite Treated with Dynamic Water. *Energy Fuels* **2014**, *28*, 1652-1663.
31. Silvestri, A.; Ataman, E.; Budi, A.; Stipp, S. L. S.; Gale, J. D.; Raiteri, P., Wetting Properties of the $CO_2$-Water-Calcite System via Molecular Simulations: Shape and Size Effects. *Langmuir* **2019**, *35*, 16669-16678.
32. Kerisit, S.; Parker, S. C., Free Energy of Adsorption of Water and Metal Ions on the {1014} Calcite Surface. *J. Am. Chem. Soc.* **2004**, *126*, 10152-10161.
33. Xiao, S.; Edwards, S. A.; Gräter, F., A New Transferable Forcefield for Simulating the Mechanics of $CaCO_3$ Crystals. *J. Phys. Chem. C* **2011**, *115*, 20067-20075.
34. Zhu, B.; Xu, X.; Tang, R., Hydration Layer Structures on Calcite Facets and Their Roles in Selective Adsorptions of Biomolecules: A Molecular Dynamics Study. *J. Chem. Phys.* **2013**, *139*, 234705.
35. Chen, H.; Eichmann, S. L.; Burnham, N. A., Understanding Calcium-Mediated Adhesion of Nanomaterials in Reservoir Fluids by Insights from Molecular Dynamics Simulations. *Sci Rep.* **2019**, *9*, 10763.
36. Raiteri, P.; Demichelis, R.; Gale, J. D., Thermodynamically Consistent Force Field for Molecular Dynamics Simulations of Alkaline-Earth Carbonates and Their Aqueous Speciation. *J. Phys. Chem. C* **2015**, *119*, 24447-24458.
37. Cygan, R. T.; Romanov, V. N.; Myshakin, E. M., Molecular Simulation of Carbon Dioxide Capture by Montmorillonite Using an Accurate and Flexible Force Field. *J. Phys. Chem. C* **2012**, *116*, 13079-13091.

38. Silvestri, A.; Budi, A.; Ataman, E.; Olsson, M. H. M.; Andersson, M. P.; Stipp, S. L. S.; Gale, J. D.; Raiteri, P., A Quantum Mechanically Derived Force Field to Predict $CO_2$ Adsorption on Calcite {10.4} in an Aqueous Environment. *J. Phys. Chem. C* **2017**, *121*, 24025-24035.
39. Berendsen, H. J. C.; Grigera, J. R.; Straatsma, T. P., The Missing Term in Effective Pair Potentials. *J. Phys. Chem.* **1987**, *91*, 6269-6271.
40. Berendsen, H. J. C.; Postma, J. P. M.; van Gunsteren, W. F.; Hermans, J., Interaction Models for Water in Relation to Protein Hydration. In *Intermolecular Forces: Proceedings of the Fourteenth Jerusalem Symposium on Quantum Chemistry and Biochemistry Held in Jerusalem, Israel, April 13–16, 1981*; Pullman, B., Ed.; Dordrecht: Springer Netherlands, 1981; pp 331-342.
41. Wu, Y.; Tepper, H. L.; Voth, G. A., Flexible Simple Point-Charge Water Model with Improved Liquid-State Properties. *J. Chem. Phys.* **2006**, *124*, 024503.
42. Jorgensen, W. L.; Chandrasekhar, J.; Madura, J. D.; Impey, R. W.; Klein, M. L., Comparison of Simple Potential Functions for Simulating Liquid Water. *J. Chem. Phys.* **1983**, *79*, 926-935.
43. Abascal, J. L. F.; Vega, C., A General Purpose Model for the Condensed Phases of Water: TIP4P/2005. *J. Chem. Phys.* **2005**, *123*, 234505.
44. Soper, A. K., The Radial Distribution Functions of Water and Ice from 220 to 673 K and at Pressures up to 400 MPa. *Chem Phys* **2000**, *258*, 121-137.
45. Mark, P.; Nilsson, L., Structure and Dynamics of the TIP3P, SPC, and SPC/E Water Models at 298 K. *J. Phys. Chem. A* **2001**, *105*, 9954-9960.
46. Le, T. T. B.; Striolo, A.; Cole, D. R., Structural and Dynamical Properties Predicted by Reactive Force Fields Simulations for Four Common Pure Fluids at Liquid and Gaseous Non-Reactive Conditions. *Mol. Simul.* **2018**, *44*, 826-839.
47. Wasserman, E.; Wood, B.; Brodholt, J., The Static Dielectric Constant of Water at Pressures up to 20 kbar and Temperatures to 1273 K: Experiment, Simulations, and Empirical Equations. *Geochim. Cosmochim. Acta* **1995**, *59*, 1-6.
48. Balasubramanian, S.; Mundy, C. J.; Klein, M. L., Shear Viscosity of Polar Fluids: Molecular Dynamics Calculations of Water. *J. Chem. Phys.* **1996**, *105*, 11190-11195.
49. Shvab, I.; Sadus, R. J., Intermolecular Potentials and the Accurate Prediction of the Thermodynamic Properties of Water. *J. Chem. Phys.* **2013**, *139*, 194505.
50. De Pablo, J. J.; Prausnitz, J. M.; Strauch, H. J.; Cummings, P. T., Molecular Simulation of Water along the Liquid–Vapor Coexistence Curve from 25 °C to the Critical Point. *J. Chem. Phys.* **1990**, *93*, 7355-7359.
51. Raabe, G.; Sadus, R. J., Molecular Dynamics Simulation of the Dielectric Constant of Water: The Effect of Bond Flexibility. *J. Chem. Phys.* **2011**, *134*, 234501.
52. Raabe, G.; Sadus, R. J., Molecular Dynamics Simulation of the Effect of Bond Flexibility on the Transport Properties of Water. *J. Chem. Phys.* **2012**, *137*, 104512.
53. Vega, C.; Abascal, J. L. F.; Nezbeda, I., Vapor-Liquid Equilibria from the Triple Point up to the Critical Point for the New Generation of TIP4P-like Models: TIP4P/Ew, TIP4P/2005, and TIP4P/Ice. *J. Chem. Phys.* **2006**, *125*, 234501.
54. Vega, C.; de Miguel, E., Surface Tension of the Most Popular Models of Water by using the Test-Area Simulation Method. *J. Chem. Phys.* **2007**, *126*, 154707.
55. González, M. A.; Abascal, J. L. F., The Shear Viscosity of Rigid Water Models. *J. Chem. Phys.* **2010**, *132*, 096101.
56. Vega, C.; Abascal, J. L. F.; Conde, M. M.; Aragones, J. L., What Ice Can Teach Us about Water Interactions: A Critical Comparison of the Performance of Different Water Models. *Faraday Discuss.* **2009**, *141*, 251-276.

57. Joung, I. S.; Cheatham III, T. E., Determination of Alkali and Halide Monovalent Ion Parameters for Use in Explicitly Solvated Biomolecular Simulations. *J. Phys. Chem. B* **2008**, *112*, 9020-9041.
58. Aragones, J. L.; Sanz, E.; Vega, C., Solubility of Nacl in Water by Molecular Simulation Revisited. *J. Chem. Phys.* **2012**, *136*, 244508.
59. Hockney, R. W.; Eastwood, J. W. *Computer Simulation Using Particles*; Taylor & Francis, N.Y., 1988.
60. Allen, M. P.; Tildesley, D. J. *Computer Simulation of Liquids*; Oxford University Press: Oxford, U.K., 2004.
61. Heine, D. R.; Grest, G. S.; Webb, E. B., Spreading Dynamics of Polymer Nanodroplets in Cylindrical Geometries. *Phys. Rev. E* **2004**, *70*, 011606.
62. Van der Spoel, D.; Lindahl, E.; Hess, B.; Groenhof, G.; Mark, A. E.; Berendsen, H. J. C., Gromacs: Fast, Flexible, and Free. *J. Comput. Chem.* **2005**, *26*, 1701-1718.
63. Hess, B.; Kutzner, C.; van der Spoel, D.; Lindahl, E., Gromacs 4: Algorithms for Highly Efficient, Load-Balanced, and Scalable Molecular Simulation. *J. Chem. Theory Comput.* **2008**, *4*, 435-447.
64. Hockney, R. W.; Goel, S. P.; Eastwood, J. W., Quiet High-Resolution Computer Models of a Plasma. *J. Comput. Phys.* **1974**, *14*, 148-158.
65. Nose, S., A Molecular Dynamics Method for Simulations in the Canonical Ensemble. *Mol. Phys.* **1984**, *52*, 255-268.
66. Hoover, W. G., Canonical Dynamics: Equilibrium Phase-Space Distributions. *Phys. Rev. A* **1985**, *31*, 1695-1697.
67. Basconi, J. E.; Shirts, M. R., Effects of Temperature Control Algorithms on Transport Properties and Kinetics in Molecular Dynamics Simulations. *J. Chem. Theory Comput.* **2013**, *9*, 2887-2899.
68. Plimpton, S., Fast Parallel Algorithms for Short-Range Molecular Dynamics. *J. Comput. Phys.* **1995**, *117*, 1-19.
69. Martyna, G. J.; Tobias, D. J.; Klein, M. L., Constant Pressure Molecular Dynamics Algorithms. *J. Chem. Phys.* **1994**, *101*, 4177-4189.
70. de Ruijter, M. J.; Blake, T. D.; De Coninck, J., Dynamic Wetting Studied by Molecular Modeling Simulations of Droplet Spreading. *Langmuir* **1999**, *15*, 7836-7847.
71. Fenter, P.; Geissbuhler, P.; DiMasi, E.; Srajer, G.; Sorensen, L. B.; Sturchio, N. C., Surface Speciation of Calcite Observed in Situ by High-Resolution X-Ray Reflectivity. *Geochim. Cosmochim.* Acta **2000**, *64*, 1221-1228.
72. Geissbühler, P.; Fenter, P.; DiMasi, E.; Srajer, G.; Sorensen, L. B.; Sturchio, N. C., Three-Dimensional Structure of the Calcite–Water Interface by Surface X-Ray Scattering. *Surf. Sci* **2004**, *573*, 191-203.
73. Heberling, F.; Trainor, T. P.; Lützenkirchen, J.; Eng, P.; Denecke, M. A.; Bosbach, D., Structure and Reactivity of the Calcite–Water Interface. *J. Colloid Interface Sci.* **2011**, *354*, 843-857.
74. Nielsen, L. C.; Bourg, I. C.; Sposito, G., Predicting $CO_2$-Water Interfacial Tension under Pressure and Temperature Conditions of Geologic $CO_2$ Storage. *Geochim. Cosmochim. Acta* **2012**, *81*, 28-38.
75. Liu, Y.; Panagiotopoulos, A. Z.; Debenedetti, P. G., Monte Carlo Simulations of High-Pressure Phase Equilibria of $CO_2$–$H_2O$ Mixtures. *J. Phys. Chem. B* **2011**, *115*, 6629-6635.
76. Orozco, G. A.; Economou, I. G.; Panagiotopoulos, A. Z., Optimization of Intermolecular Potential Parameters for the $CO_2$/$H_2O$ Mixture. *J. Phys. Chem. B* **2014**, *118*, 11504-11511.

77. Vlcek, L.; Chialvo, A. A.; Cole, D. R., Optimized Unlike-Pair Interactions for Water-Carbon Dioxide Mixtures Described by the SPC/E and EPM2 Models. *J. Phys. Chem. B* **2011**, *115*, 8775-8784.
78. Myshakin, E. M.; Saidi, W. A.; Romanov, V. N.; Cygan, R. T.; Jordan, K. D., Molecular Dynamics Simulations of Carbon Dioxide Intercalation in Hydrated Na-Montmorillonite. *J. Phys. Chem. C* **2013**, *117*, 11028-11039.
79. Fenter, P.; Sturchio, N. C., Calcite (1 0 4)–Water Interface Structure, Revisited. *Geochim. Cosmochim. Acta* **2012**, *97*, 58-69.
80. Lardge, J. S.; Duffy, D. M.; Gillan, M. J.; Watkins, M., Ab Initio Simulations of the Interaction between Water and Defects on the Calcite $(10\bar{1}4)$ Surface. *J. Phys. Chem. C* **2010**, *114*, 2664-2668.
81. Liu, J.; Wani, O. B.; Alhassan, S. M.; Pantelides, S. T., Wettability Alteration and Enhanced Oil Recovery Induced by Proximal Adsorption of $Na^+$, $Cl^-$, $Ca^{2+}$, $Mg^{2+}$, and $SO_4^{2-}$ Ions on Calcite. *Phys. Rev. Appl.* **2018**, *10*, 034064.
82. Wolthers, M.; Di Tommaso, D.; Du, Z.; de Leeuw, N. H., Calcite Surface Structure and Reactivity: Molecular Dynamics Simulations and Macroscopic Surface Modelling of the Calcite-Water Interface. *Phys. Chem. Chem. Phys.* **2012**, *14*, 15145-15157.
83. Reischl, B.; Raiteri, P.; Gale, J. D.; Rohl, A. L., Atomistic Simulation of Atomic Force Microscopy Imaging of Hydration Layers on Calcite, Dolomite, and Magnesite Surfaces. *J. Phys. Chem. C* **2019**, *123*, 14985-14992.
84. Buckley, J. S.; Takamura, K.; Morrow, N. R., Influence of Electrical Surface Charges on the Wetting Properties of Crude Oils. *SPE Res. Eng.* **1989**, *4*, 332-340.
85. Koleini, M. M.; Mehraban, M. F.; Ayatollahi, S., Effects of Low Salinity Water on Calcite/Brine Interface: A Molecular Dynamics Simulation Study. *Colloid Surf. A* **2018**, *537*, 61-68.
86. Argyris, D.; Cole, D. R.; Striolo, A., Ion-Specific Effects under Confinement: The Role of Interfacial Water. *ACS Nano* **2010**, *4*, 2035-2042.
87. Ho, T. A.; Argyris, D.; Cole, D. R.; Striolo, A., Aqueous NaCl and CsCl Solutions Confined in Crystalline Slit-Shaped Silica Nanopores of Varying Degree of Protonation. *Langmuir* **2012**, *28*, 1256-1266.

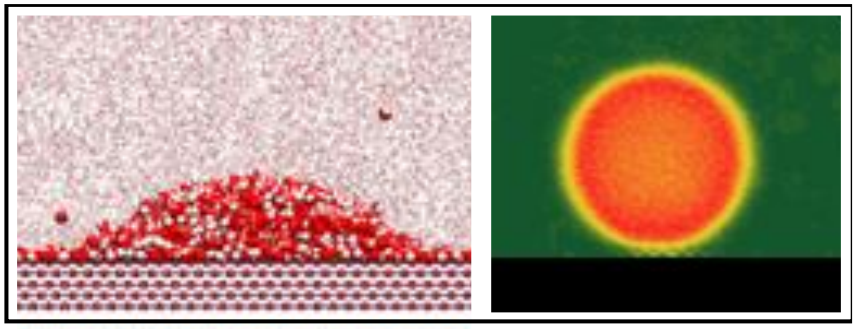

Table of Contents figure.